Proceedings of the
Annual Stability Conference
Structural Stability Research Council
San Antonio, Texas, March 19-22, 2024

Understanding the behavior of built-up cold-formed steel lightweight concrete (CFS-LWC) composite beams

Rohola Rahnavard[1], Hélder D. Craveiro [2], Rui A. Simões[3], Shahabeddin Torabian [4], Benjamin W. Schafer [5]

Abstract

Recent experimental and numerical studies have shown that mobilizing composite action within systems comprising cold-formed steel beams (CFS) and lightweight concrete (LWC) is feasible and can substantially improve structural performance. Moreover, the solutions under development target ease of assembly and disassembly, allowing the separation of the structural components without destructive operations. However, several issues must be investigated due to the reduced thickness of the steel profiles, hence the higher susceptibility to local buckling phenomena at the bolts acting as shear connectors. This brings extra complexity and requires new design rules for the design of CFS-LWC composite beams, assessing in detail the attained composite action using bolts as shear connectors. Designing CFS-LWC composite beams depends on determining the degree of shear connection, for which the available design codes present formulas to predict shear resistance for welded shear studs; however, their applicability to the case of bolted shear connectors is still unclear. Moreover, the available design procedures are specified for normal concrete (with a density higher than 1750 kg/m^3) and limited for lightweight concrete (LWC); this is therefore the focus of this study. This study uses numerical modeling to assess the structural behavior of innovative built-up CFS-lightweight concrete (LWC) demountable composite beams using bolted shear connectors. First, numerical simulations of the CFS-LWC composite beam and bolted shear connectors are proposed and calibrated against existing experimental results. The CFS-LWC composite beams with different degrees of shear connection are then simulated, and their results are compared with design predictions following AISC 360, assessing the design suitability.

Keywords

[1] Pd.D. candidate, *University of Coimbra, ISISE, ARISE, Department of Civil Engineering, Coimbra, Portugal*, <rahnavard@uc.pt>
[2] Researcher, *University of Coimbra, ISISE, ARISE, Department of Civil Engineering, Coimbra, Portugal*, < heldercraveiro.eng@uc.pt >
[3] Associate Professor, *University of Coimbra, ISISE, ARISE, Department of Civil Engineering, Coimbra, Portugal*, <rads@uc.pt>
[4] Researcher, *Johns Hopkins University, Baltimore, MD, United States of America*, < storabian@sgh.com >
[5] Professor, *Johns Hopkins University, Baltimore, MD, United States of America*, < schafer@jhu.edu >

Built-up section; cold-formed steel; composite beam; buckling; lightweight concrete; bolted shear connector

1. Introduction

The application of cold-formed steel (CFS) in construction is being increased due to its high versatility and suitable strength-to-weight ratio. Recent studies showed the feasibility of applying cold-formed steel (CFS) members in composite systems (Rahnavard et al., 2022). The use of CFS sections in composite flooring systems with wood-based boards has been investigated. Xu and Tangorra investigated the serviceability performance of typical flooring systems comprising CFS-lipped channel joists and wood-based boards. Kyvelou et al. studied the effect of the degree of shear connection between CFS joists and wood-based flooring panels on their bending capacity, concluding that the fasteners' spacing significantly influenced the system's moment capacity and flexural stiffness.

The use of CFS section in composite beam systems leads to lower construction time and cost. The neutral axis in composite beams can be raised from the beam centroid towards the concrete slab by combining the CFS beam with a concrete slab, which would lead to putting more of the steel member in tension, resulting in more optimized use of steel in tension and concrete in compression (Rahnavard et al. 2023). Reducing compression stress on the beam could reduce the buckling potentials of the CFS beams as well; this would be a more sustainable option due to the reduced material consumption. In this scenario, composite beam concrete and CFS components are utilized to their maximum potential. The built-up CFS cross-sections suit this purpose due to their geometric diversity. In other words, the CFS section's buckling sensitivity could be solved if it acts predominantly in tension, allowing nearly full plasticization of the cross-section in the ultimate load condition. Although the CFS built-up sections have these advantages, most current building regulations still do not address using CFS sections in composite construction. At the same time, very minimal research has been conducted to investigate composite beams comprising CFS built-up and LWC slabs. In this paper, a finite element model is validated versus recently conducted experimental studies by the authors (Rahnavard et al. 2023) to simulate the behavior of built-up CFS-LWC composite beams and to further analyze their behavior. The focus is initially to provide a reliable simulation by defining accurate material properties, boundary conditions, and interactions. A parametric study is then presented, and its results are compared with the prediction following AISC-360.

2. Numerical study

In this section, the available experimental study conducted by the authors is first briefly described. Four full-scall experimental specimens of built-up cold-formed steel lightweight concrete (CFS-LWC) composite beams, including two built-up CFS configurations and two different degrees of shear connections tested by authors (Rahnavard et al. 2023), are selected for verification purposes herein. According to experimental study (Rahnavard et al. 2023), the selected composite beams were (a) 2C-P1: CFS built-up cross-section comprising two-lipped channels fastened back-to-back and with a partial shear connection between the concrete slab and CFS built-up beam using 40 bolted shear connectors, (b) 2C-P2: CFS built-up cross-section comprising two-lipped channels fastened back-to-back and with a partial shear connection between the concrete slab and CFS built-up beam using 20 bolted shear connectors, (c) 2C+C-P1: CFS built-up cross-section comprising

two-lipped channels fastened back-to-back stiffened with another lipped channel attached to the bottom flanges with a partial shear connection between the concrete slab and CFS built-up beam using 40 bolted shear connectors, and (d) 2C+C-P2: CFS built-up cross-section comprising two-lipped channels fastened back-to-back stiffened with another lipped channel attached to the bottom flanges with a partial shear connection between the concrete slab and CFS built-up beam using 20 bolted shear connectors. More details regarding the specimens and tests can be found in (Rahnavard et al. 2023).

In this study, different profile geometry is used for lipped channels fastened back-to-back and C-137×62×17×2.5 for the stiffened profile, as shown in Fig. 1. The CFS profile height varies from 240 mm to 300 mm (240, 260, 280, and 300 mm). Fig. 2 shows the details of the CFS-LWC composite beams, in which the concrete thickness h_c varies, including 85 mm, 100 mm, and 115 mm. The length of the CFS fabricated beams is 4910 mm for all models. The steel deck is 4600 mm in length and 1075 mm in width for all models. The composite beam's effective length is 4300 mm (support to support distance). M16 8.8 bolts (d_s=16 mm) are used as shear connectors to attach the CFS built-up beams to the flooring system, as shown in Fig 2. Two lightweight concrete grades, including 25 MPa and 35 MPa, with a density ρ of 1850 kg/m^3 are considered. The CFS-LWC models are investigated under a four-point bending setup, as shown in Fg.3. Table 1 lists the details of the 48 models used in this study.

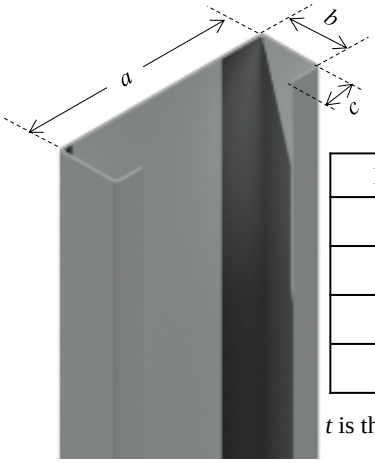

Dimension	C1	C2
a (mm)	240-300	137
b (mm)	65	62
c (mm)	20	17
t (mm)	2.5	2

t is the thickness of the profile.

Figure 1: The CFS-lipped channel details (dimension in mm).

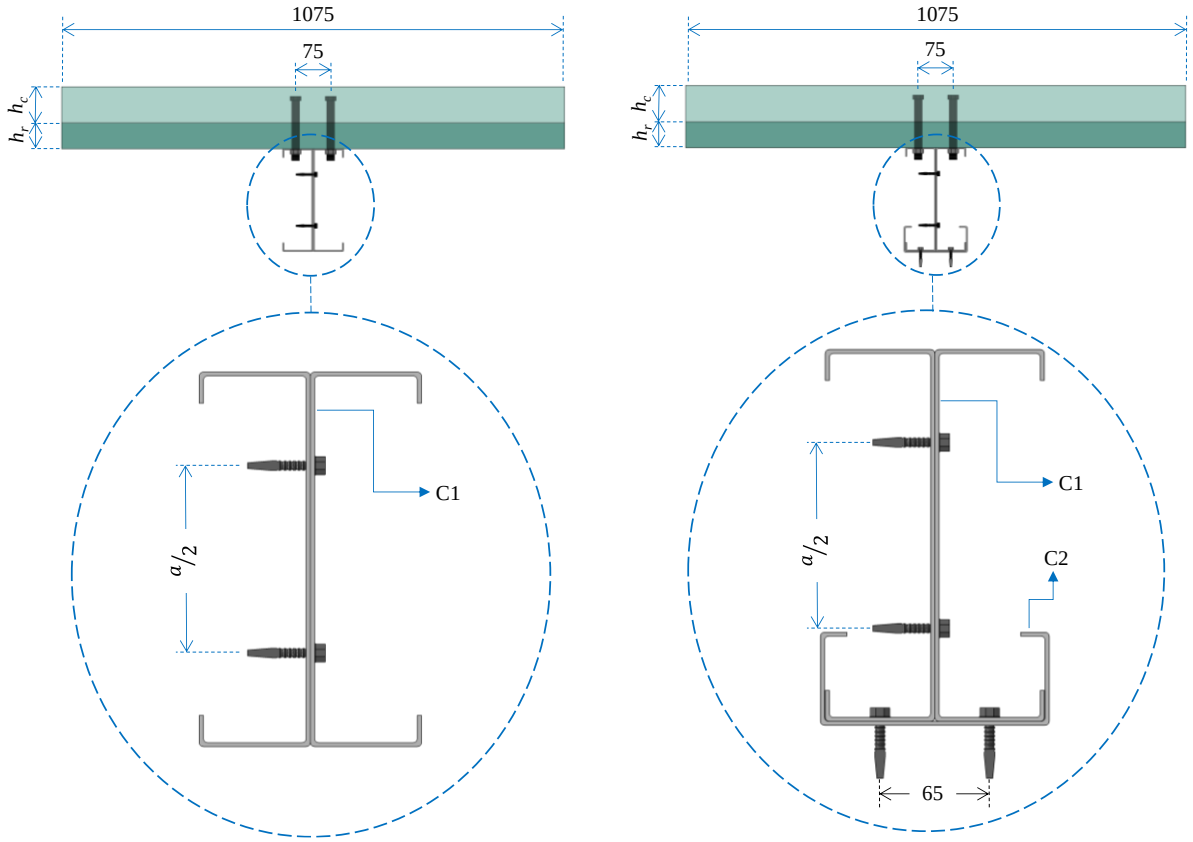

a) CFS-LWC composite section with two back-to-back lipped channels

CFS-LWC composite section with two back-to-back lipped channels and strengthened on the bottom flange with another lipped channel

Figure 2: CFS-LWC cross-sections (dimension in mm).

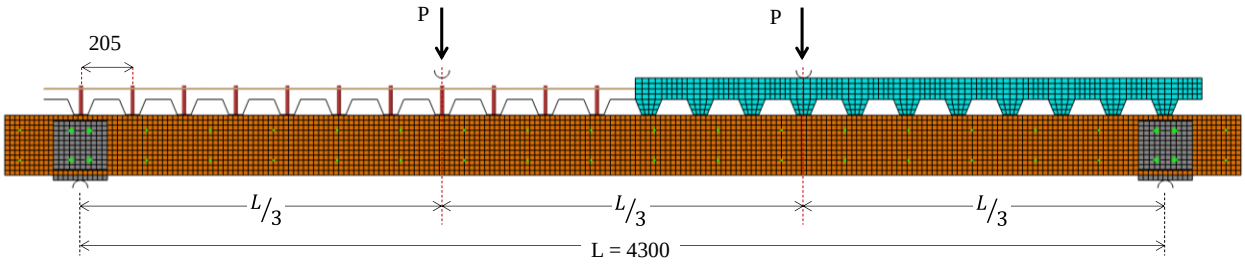

Figure 3: Geometry details of CFS-LWC composite beam (dimension in mm).

Table 1: The model specifications.

Group ID	a (mm)	*CFS sections*	f_c (MPa)	L (mm)	h_r (mm)	h_c (mm)
2C-h85-fc25	240, 260, 280 and 300	2C1	25	4300	60	85
2C-h100-fc25	240, 260, 280 and 300	2C1	25	4300	60	100
2C-h115-fc25	240, 260, 280 and 300	2C1	25	4300	60	115
2C-h85-fc35	240, 260, 280 and 300	2C1	35	4300	60	85
2C-h100-fc35	240, 260, 280 and 300	2C1	35	4300	60	100

2C-h115-fc35	240, 260, 280 and 300	2C1	35	4300	60	115
2C+C-h85-fc25	240, 260, 280 and 300	2C1+C2	25	4300	60	85
2C+C-h100-fc25	240, 260, 280 and 300	2C1+C2	25	4300	60	100
2C+C-h115-fc25	240, 260, 280 and 300	2C1+C2	25	4300	60	115
2C+C-h85-fc35	240, 260, 280 and 300	2C1+C2	35	4300	60	85
2C+C-h100-fc35	240, 260, 280 and 300	2C1+C2	35	4300	60	100
2C+C-h115-fc35	240, 260, 280 and 300	2C1+C2	35	4300	60	115

2.1 Concrete material properties

This study uses Abaqus's concrete damage plasticity model (CDP). Modulus of elasticity, Poisson's ratio, plasticity parameters, compressive and tensile behavior are needed to simulate the concrete using the CDP model. As mentioned, two concrete grades are used in this study with cylindrical strengths f_{lcm} of 25 MPa and 35 MPa with a density ρ of 1850 kg/m^3. Therefore, the modulus of elasticity E_{lcm}, compressive stress-strain curve $\sigma_c - \varepsilon_c$, and tensile stress-strain curve $\sigma_t - \varepsilon_t$ are then defined. Eq.1 is used to determine the modulus of elasticity E_{lcm} of lightweight concrete, as proposed by Aslani and Jowkarmeimandi, 2012.

The concrete behavior in compression is modeled linearly up to 40% of the compressive strength f_{lcm} (OA in Fig.4a) according to EN 1992-1-1 and the concrete model proposed by Aslani and Jowkarmeimandi, 2012. Eq.2 is then used to define the plastic behavior up to the nominal ultimate strain ε_{lcu1} of 0.0035 (ABC in Fig.4a). An extension is then defined for the compressive behavior of lightweight concrete after reaching the nominal ultimate strain (CD in Fig.4a) following Eq.2 **Error! Reference source not found.**. In Eq.2, the parameter n is calculated using Eq.3. The compression damage variable d_c is considered for concrete. Eq.4 defines the damage variable vs. crushing strain curve (Fig.4b).

The uniaxial tensile stress is required to define the tensile behavior of concrete in the CDP model. The concrete behavior in tension is linear up to the maximum tensile strength f_{lctm} and then drops. The maximum tensile strength f_{lctm} is determined using Eq.5. Eqs. 6-8 are used to define the softening part of the tensile stress-strain curve. In Eqs 6, w is the plastic displacement, c_1 is 3.0, c_2 is 6.93, and the cracking width(w_c can be calculated using Eq.6, where fracture energy can be obtained by Eq.7, suggested by FIB. Therefore, Eq.8 determines the strain as a function of crack opening (Fig.4c). The tensile damage variable (d_t) is considered for concrete. The damage variable vs. cracking strain curve is defined according to Eq.9. Fig.4d shows the tensile stress and damage variable versus strain relationship.

$$E_{lcm} = (3320\sqrt{f_{lcm}} + 6900) \times (\frac{\rho}{2320})^{1.5} \quad (1)$$

$$\sigma_c = \frac{n\left(\frac{\varepsilon_c}{\varepsilon_{lc1}}\right) f_{lcm}}{n-1+\left(\frac{\varepsilon_c}{\varepsilon_{lc1}}\right)^n} \quad (2)$$

$$n = \begin{cases} n_1 = \left(1.02 - 1.17\frac{f_{lcm}}{E_{lcm}\varepsilon_{lc1}}\right)^{-0.74} & \varepsilon_c \le \varepsilon_{lc1} \\ n_1 + (3.5 \times (12.4 - 0.0166 f_{lcm})^{-0.46}) + 23.24 e^{-911/f_{lcm}} & \varepsilon_c > \varepsilon_{lc1} \end{cases} \quad (3)$$

$$d_c = 1 - \frac{\sigma_c}{f_{lcm}} \tag{4}$$

$$f_{lctm} = 0.3 \times (0.4 + \frac{0.6\rho}{2200}) f_{lck}^{\ 2/3} \tag{5}$$

$$\sigma_t = f_{lctm} \times \left[\left(1 + (\frac{3w}{w_c})^3\right) e^{-\frac{6.93w}{w_c}} - \frac{w}{w_c}(1+3^3)e^{-6.93} \right], w_c = {5.14 \times 73 f_{lcm}^{\ 0.18}}/{f_{lctm}} \tag{6}$$

$$G_f = 73 f_{lcm}^{\ 0.18} \tag{7}$$

$$\varepsilon_t = \frac{f_{lctm}}{E_{lc0}} + \frac{w}{l_{eq}} \tag{8}$$

$$d_t = 1 - \frac{\sigma_t}{f_{lctm}} \tag{9}$$

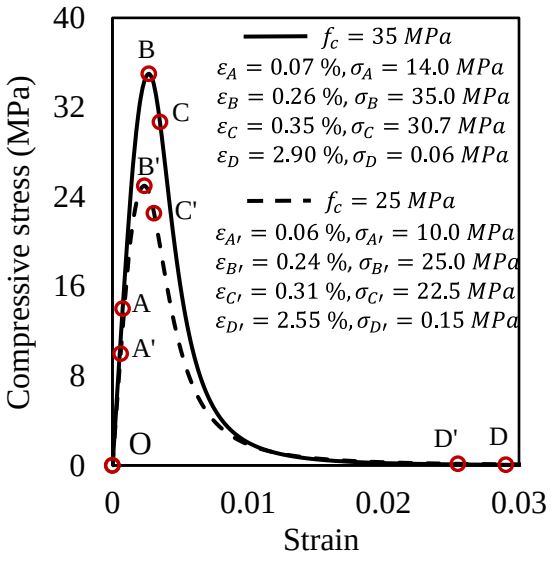

(a) Compressive stress versus strain relationship

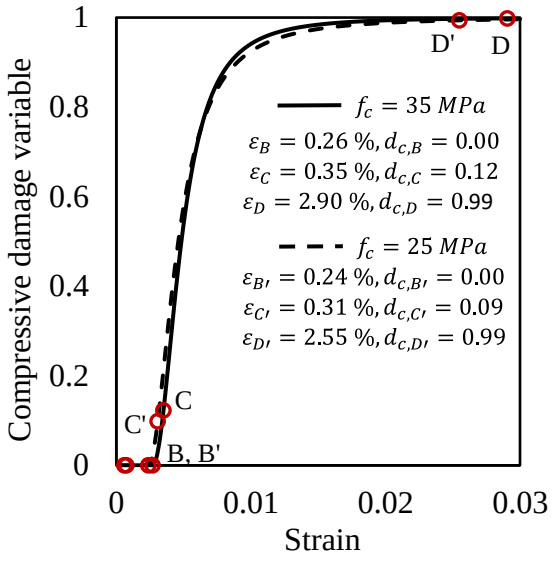

(b) compressive damage variable versus strain relationship

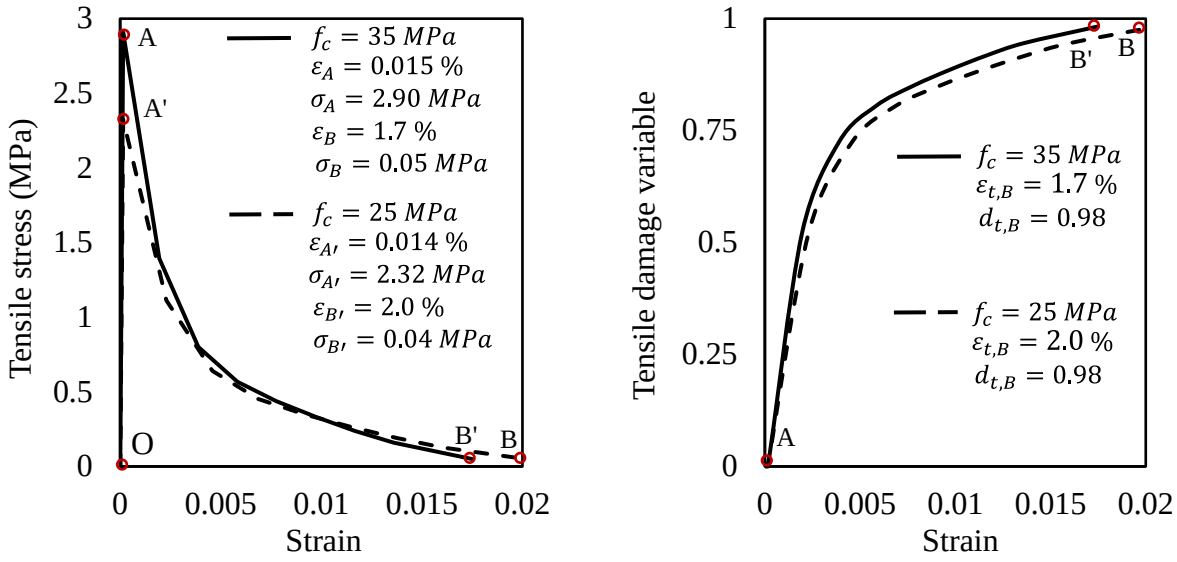

(c) Tensile stress versus strain relationship

(d) Tensile damage variable versus strain relationship

Figure 4: Lightweight concrete behavior.

2.2 Steel material properties

The CFS material properties are defined in an elastic and plastic range using the available options in Abaqus. The elastic modulus of 204 GPa and a Poisson's ratio of 0.3 is defined for the CFS sections according to the tensile test results (Rahnavard et al., 2023). The plastic stress-strain curve is converted from the engineering stress-strain curve and defined for the plastic behavior of the CFS sections. Fig. 6 shows the true and engineering stress-strain curve for structural steel grade S280GD+Z. Similarly, the elastic behavior of bolted shear connectors and reinforcement is introduced by defining an elastic modulus of 200 GPa and a Poisson's ratio of 0.3. The plastic behavior is defined using bilinear according to the nominal yield f_{yb} of 640 MPa and ultimate stress f_{ub} of 800 MPa. Moreover, reinforcement mesh with a diameter of 8 mm, spacing of 150 mm, and yield stress of 500 MPa are used.

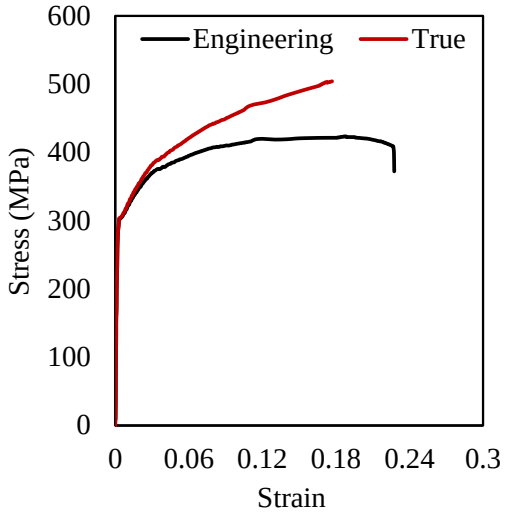

Figure 5: Stress-strain curve for structural steel grade S280GD+Z.

2.3 Boundary condition, meshing, and interaction

Fig. 6 shows the finite element modeling of the CFS-LWC composite beam. As can be seen, the loading system is modeled using two loading parts, which RP-1 and RP-2 represent them. RP-1 and RP-2 are then coupled to the RP-3 coupling beam type. The RP-3 can move in the z-direction, and the rest of the translational and rotational degrees of freedom were fixed.

Fig. 6 shows that steel plates are used to enhance the CFS web in the support region against shear stress. These steel plates are connected to the CFS profiles using beam connectors. The simply supports are modelled using a solid plate with a thickness of 20 mm and a rigid element. RP-4 and RP-5 represent left and right rigid parts, respectively, and are fixed in all rotational and transitional directions. S4R elements are used to simulate CFS profiles, the steel plates for supporting the CFS web, and the steel deck. C3D8R element is used to simulate the support plates and the concrete slab. B31 beam element is used to simulate the bolted shear connector and the reinforcements.

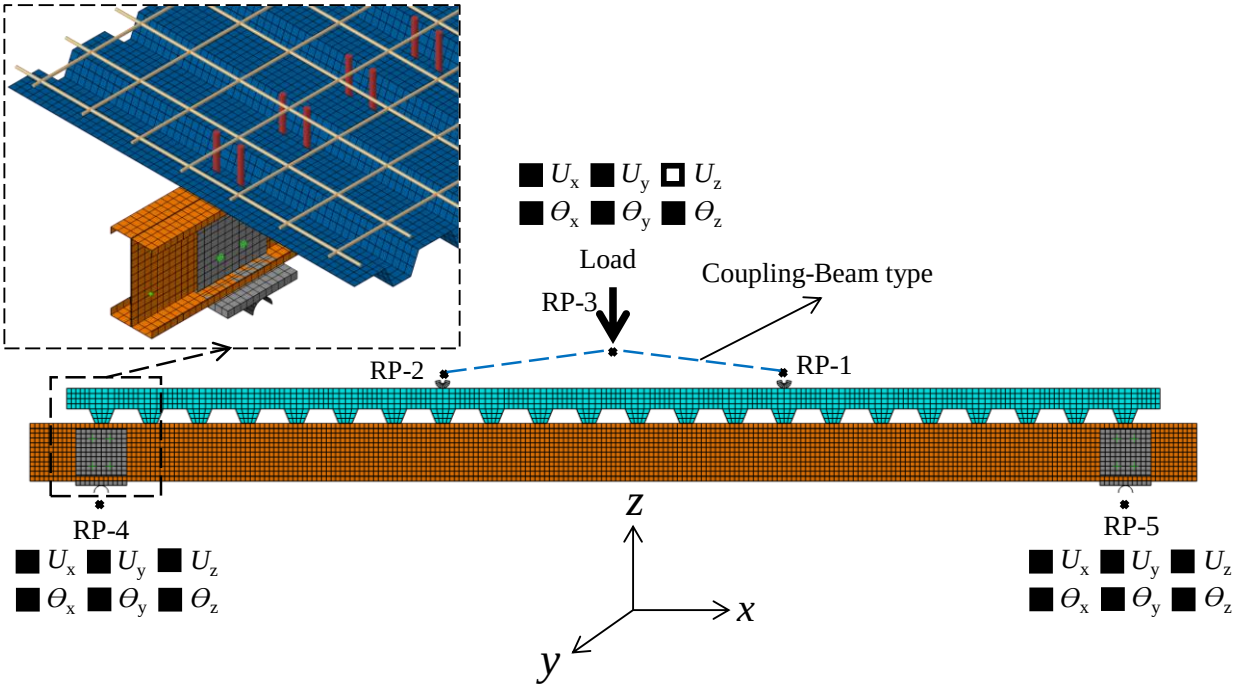

Figure 6: Finite element modeling of the CFS-LWC composite beam.

2.4 Verification

The developed finite element models are verified against the results of four tests performed on composite beam systems comprising cold-formed steel beams and lightweight concrete; a detailed description of these experiments can be found in (Rahnavard et al. 2023). Two built-up CFS sections were employed in the tests, along with two different numbers of shear connectors: two rows of shear connectors along the beam with ten shear connectors in each row (2C-P1 and 2C+C-P1) and two rows of shear connectors along the beam with twenty shear connectors in each row (2C-P2 and 2C+C-P2). A typical cross-section of the tested flooring systems is shown in Fig.2.

The comparison of the load-deflection responses of the tested and simulated CFS-LWC composite systems, as illustrated in Fig.7. The results show a close agreement between tests and models.

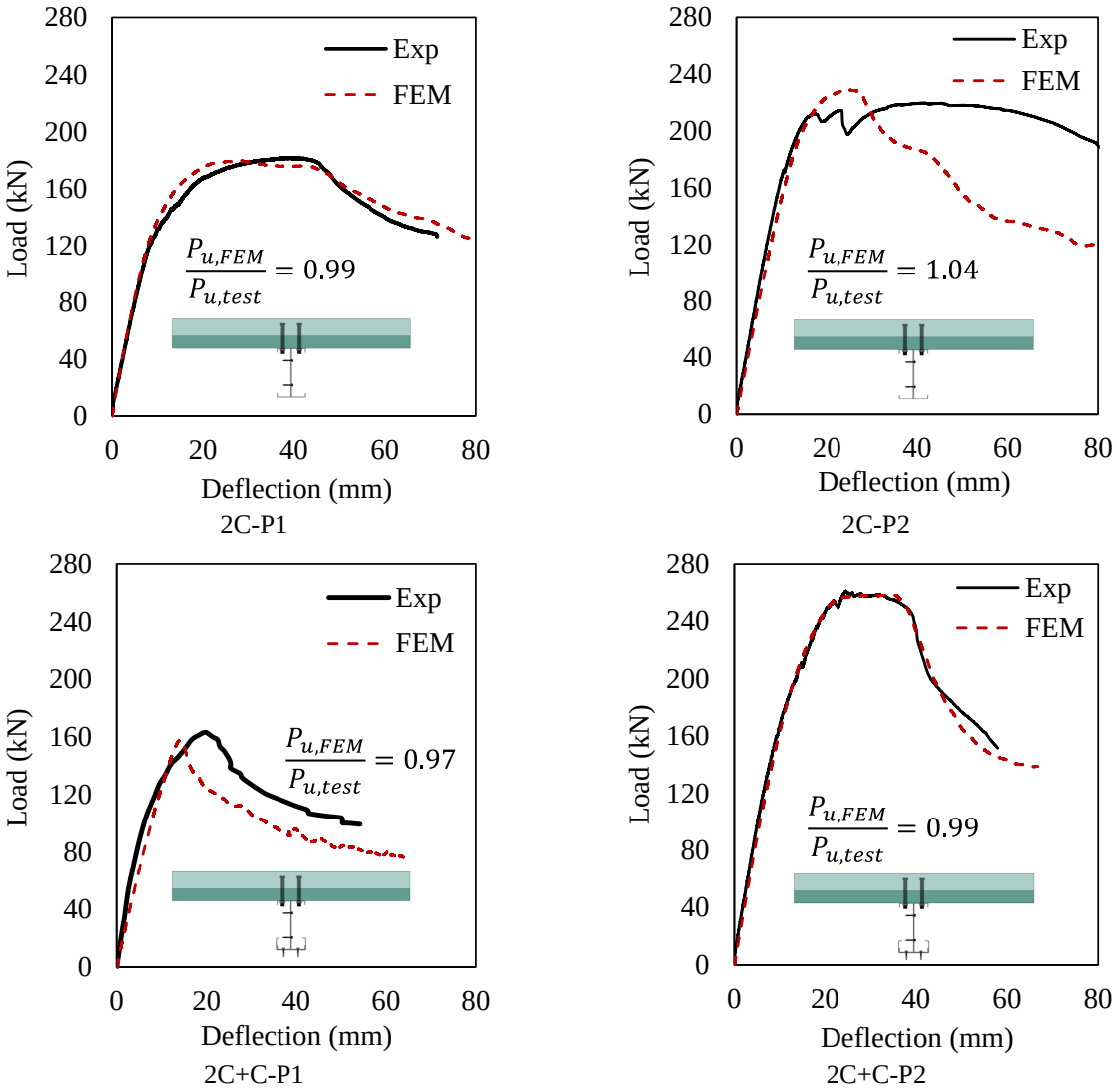

Figure 7: Comparison of load-deflection curves of CFS-LWC composite beam tested by Rahnavard et al. 2023 and simulated herein.

3. Design prediction following AISC-360

The moment capacity of a composite cold-formed steel lightweight concrete flooring system obtained from the modeling is compared with the design prediction following AISC-360. The generated shear force in the interface of the lightweight concrete and CFS built-up steel is the minimum value of the tensile strength of the CFS built-up steel beam $N_{pl,a}$ and the compressive strength of the concrete slab $N_{c,Rd}$ (Eq. 10), where b_{eff} is the effective width and is one-fourth of the beam span (center-to-center of supports) (AISC-360).

Therefore, for a flooring system with n_c connectors in the critical lengths, the attained degree of shear connection (η_d) is given by Eq. 11. In Eq. 11, N_c is the design value of the compressive force in the concrete flange. In Eq.11, P_{Rd} is the shear strength of the shear connectors or the bearing

resistance of the concrete slab in contact with the shear connectors, determines the maximum longitudinal force that may be sustained and transferred by the shear connector of a composite beam, and is calculated by Eq.12. In Eq. 12, the group effect factor (R_g) is 0.85, and the stud position factor (R_P) is 0.6 for the two steel-headed stud anchors connected to the steel deck rib, with the deck oriented perpendicular to the steel shape, as suggested by AISC-360. In Eq.12, the modulus of elasticity is obtained using Eq.13, as suggested by AISC-360.

$$N_{c,f} = min\left(N_{pl,a} = f_y A_a, N_{c,Rd} = 0.85 f_{lcm} b_{eff} h_c\right) \tag{10}$$

$$\eta_d = \frac{N_c}{N_{c,f}} = \frac{n_c \times P_{Rd}}{N_{c,f}} \leq 1 \tag{11}$$

$$P_{Rd} = min\left(\frac{0.5\pi {d_s}^2 \sqrt{f_{lcm} E_{lcm,AISC}}}{4}, \frac{R_g R_P \pi {d_s}^2 f_{ub}}{4}\right) \tag{12}$$

$$E_{lcm} = 0.043 \rho^{1.5} \sqrt{f_{lcm}} \tag{13}$$

Fig. 8 compares the moment capacity of a composite cold-formed steel lightweight concrete flooring system obtained from the modeling with the design prediction following AISC-360. The results show that the design predictions following AISC-360 overpredict the capacity of CFS-LWC up to 17% on average (COV = 2.29%) for 2C configuration and up to 35% on average (COV = 2.29%). The unconservative prediction is due to the overprediction of the shear strength of the connectors. Previous experimental studies (Ataei et al. 2023) also showed that the AISC-360 expression for the shear studs overpredicts the shear capacity for the bolted shear connector. This is the reason that leads to the results being overpredicted.

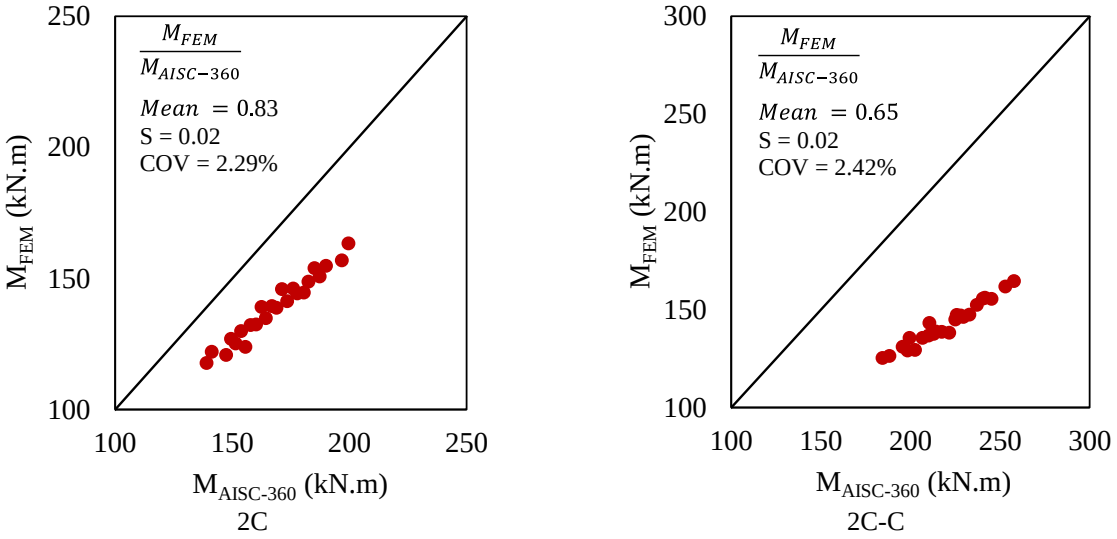

Figure 8: Comparison between the values of flexural capacity predicted by AISC-360 and FEM.

Therefore, the shear connector resistance is determined directly from the pushout modeling. The full details of the modeling details are available in the literature (Rahnavard et al., 2023). The pushout setup was considered following Annex E in EN 1994-1-1. The shear resistance of each shear connector with a diameter of 16 mm is obtained as 17.5 kN and 20.2 kN for the pushout

model with lightweight concrete grade f_c = 25 MPa and f_c = 35 MPa, respectively. The results are then updated by replacing the shear resistance obtained from the AISC-360 expression with those obtained from FEM, as shown in Fig. 9. The results show that the flexural capacity predicted by AISC-360 incorporated with the modified shear resistance obtained from FEM matches the flexural capacity obtained from the simulation for 2C configuration. However, it can be seen that for the CFS-LWC with 2C+C configurations, the design prediction is still slightly unconservative.

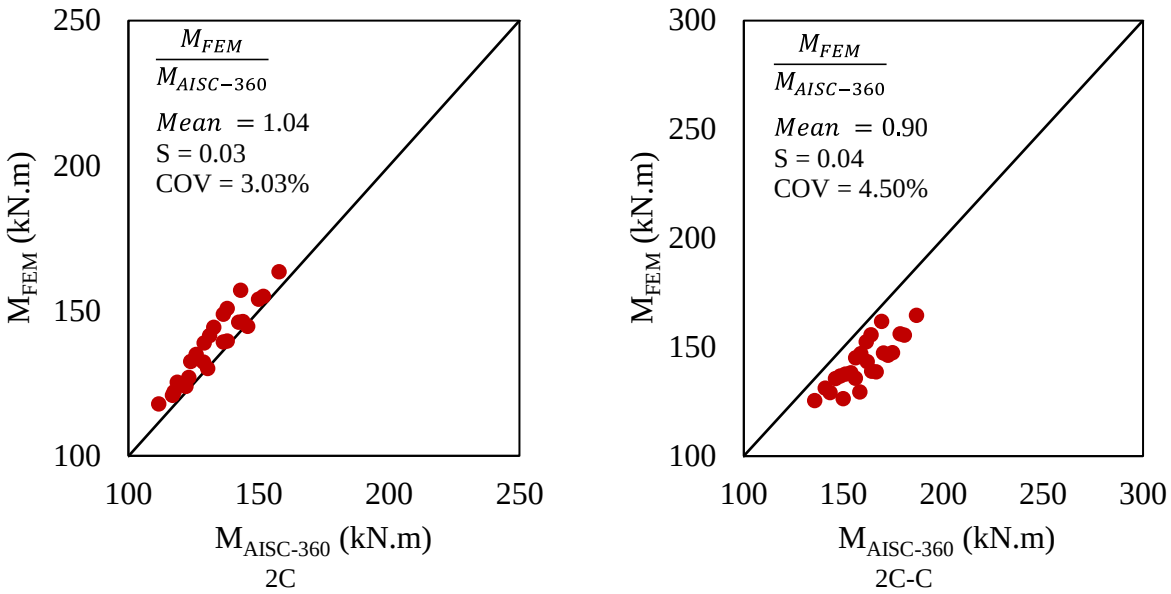

Figure 9: Comparison between the values of flexural capacity predicted by AISC-360 and modified shear resistance obtained from FEM.

4. Conclusions

A parametric study to analyze further the behavior of the CFS-LWC composite beams has been presented in this paper. The detailed modeling techniques to simulate lightweight concrete and cold-formed steel were studied. The modeling techniques were verified against the test results, resulting in a close agreement. A parametric study was investigated, including two built-up CFS section configurations, two concrete grades, three concrete slab thicknesses, and four CFS section heights. The result was then compared with design prediction following AISC-360. The result showed that the design prediction following AISC does not apply to predicting the CFS-LWC composite beam's flexural capacity. This was because the design methodology in AISC-360 is for composite beams with compact and non-compact steel sections, which are connected to the concrete slab using welded shear studs, while in CFS-LWC concrete, the CFS sections are slender, and the bolts are used as the shear connector. Therefore, the shear resistance was obtained directly from the pushout models. Finally, the flexural resistance of the CFS-LWC beams obtained from the FEM was compared with the design prediction using AISC-360 incorporated with the shear resistance obtained from the FEM, resulting in a close agreement.

Acknowledgments

This work is financed by national funds through FCT - Foundation for Science and Technology, under grant agreement 2021.06528.BD attributed to the 1st author and under the grant agreement 2020.03588.CEECIND attributed to the 2nd author.

The authors gratefully acknowledge the financial support in the scope of the Ignition and/or Proof-of-Concept project D_INNOCFSCONC – "Demonstração de solução estrutural híbrida inovadora com recurso a aço-enformado a frio e betão-leve", provided by the UI-Transfer project with reference 181315 (POCI-01-0246-FEDER-181315) and the Portuguese Foundation for Science and Technology (FCT) for its support under the framework of the research project PTDC/ECI-EGC/31858/2017 - INNOCFSCONC - Innovative hybrid structural solutions using cold-formed steel and lightweight concrete", financed by FEDER funds through the Competitivity Factors Operational Programme-COMPETE and by national funds through FCT. This work was partly financed by FCT/MCTES through national funds (PIDDAC) under the R&D Unit Institute for Sustainability and Innovation in Structural Engineering (ISISE), under reference UIDB/04029/2020, and under the Associate Laboratory Advanced Production and Intelligent Systems ARISE under reference LA/P/0112/2020.

References

Rahnavard, R., Craveiro, H.D., Lopes, M., Simões, R.A., Laím L., Rebelo, C. (2022). "Concrete-filled cold-formed steel (CF-CFS) built-up columns under compression: Test and design." *Thin-Walled Structures*, Volume 179, 109603.

Rahnavard, R., Craveiro, H.D., Simões, R.A. (2023). "Analytical prediction of the axial capacity of concrete-filled cold-formed steel (CF-CFS) built-up columns." *SSRC stability conference*.

Rahnavard, R., Craveiro, H.D., Simões, R.A., Laím L., Santiago, A. (2022). "Buckling resistance of concrete-filled cold-formed steel (CF-CFS) built-up short columns under compression." *Thin-Walled Structures*, Volume 170, 108638.

Xu, L., Tangorra, F.M. (2007). "Experimental investigation of lightweight residential floors supported by cold-formed steel C-shape joists." *Journal of Constructional Steel Research*, Volume 63, Issue 3.

Kyvelou, P., Gardner, L., Nethercot, D.A. (2017). "Testing and Analysis of Composite Cold-Formed Steel and Wood−Based Flooring Systems." *Journal of Structural Engineering*, Volume 143, Issue 11.

Rahnavard, R., Craveiro, H.D., Simões, R.A., Laím L., Santiago, A. (2023). "Test and design of built-up cold-formed steel-lightweight concrete (CFS-LWC) composite beams." *Thin-Walled Structures*, Volume 191, 111211.

Rahnavard, R., Craveiro, H.D., Simões, R.A., Torabian, S., Schafer, B.W. (2023). "Built-Up Cold-Formed Steel Lightweight Concrete (CFS-LWC) Composite Beams: Simulation And Design." *11th International Conference of Thin-Walled Structures*. Sydney.

ANSI/AISC 360-16, (2016). "Specification For Structural Steel Buildings." *American Institute of Steel Construction*, Chicago.

Abaqus Analysis User's Guide. (2017). Version 6.17 Dassault Systèmes Simulia, USA.

Aslani, F., Jowkarmeimandi, R., (2012). "Stress–strain model for concrete under cyclic loading," *Magazine of Concrete Research*, 64 (8), pp. 673-685.

EN 1992-1-1, Eurocode 2. (2010). "Design of Concrete Structures - Part 1-1: General Rules and Rules For Buildings."

CEB-FIP model code. (2010). Fib Model Code For Concrete Structures 2010. Doc Competence Cent Siegmar Kästl.

Ataei, A., Mohamoudy, S.A., Zeynalian, M., Chiniforush, A.A., Ngo, T.D. (2023). "Experimental study of innovative bolted shear connectors in demountable cold-formed steel–concrete composite beams." *Thin-Walled Structures*, Volume 192, 111112.

Rahnavard, R., Craveiro, H.D., Simões, R.A., Torabian, S., Schafer, B.W. (2023). "Evaluation of bolted shear connector used in cold-formed steel lightweight concrete (CFS-LWC) composite beams." *13th International Conference of Advances in Steel Structures*. Kuching.

EN 1994-1-1, Eurocode 4. (2004). "Design of Composite Steel and Concrete structures, Part 1.1: General Rules and Rules For building."